INTERNATIONAL JOURNAL OF INTEGRATED ENGINEERING
ISSN: 2229-838X e-ISSN: 2600-7916

IJIE

Vol. 16 No. 8 (2024) 227-235
https://publisher.uthm.edu.my/ojs/index.php/ijie

Surface Characterization of Porous Ti-6Al-4V Dental Implant by Metal Injection Molding with Palm Stearin Binder System

J. B. Saedon[1], N. H. Mohamad Nor[1]*, M. H. Ismail[1], M. Newishy[2] & Hazran Husain[1]

[1] *School of Mechanical Engineering, College of Engineering, Universiti Teknologi MARA, 40450 Shah Alam, Selangor, MALAYSIA*

[2] *Central Metallurgical Research Institute, Elfelezat Street, El-Tebbin, Helwan, 11421 Cairo, EGYPT*

*Corresponding Author: norhafiez@uitm.edu.my
DOI: https://doi.org/10.30880/ijie.2024.16.08.023

Article Info

Received: 3 July 2024
Accepted: 24 October 2024
Available online: 30 December 2024

Keywords

Porous Ti-6Al-4V, dental implant, metal injection molding (MIM), palm stearin

Abstract

The osseointegration rate of Ti-6Al-4V dental implants is related to their composition and surface roughness. Rough-surfaced implants favour both bone anchoring and biochemical stability. This paper focused on the surface characteristic of highly porous Ti-6Al-4V dental implant by metal injection molding with palm stearin binder system with an addition of sodium chloride as space holder which has been established in the fabrication of porous Ti-6Al-4V. The integrated pores obtained on the dental implant provides the space for mineralized bone to growth and diffuse into the dental implant and improve the anchorage of the dental implant towards the bone and prevent dental implant loosening. The average surface roughness (Ra) of 4.62 ± 1.33 μm and 5.83 ± 1.25 μm was within the proposed ideal surface roughness of 1-10μm. In addition, the existence of lamellar of α-β phase on the surface as-polished dental implant would improve both the mechanical as well as the elastic properties.

1. Introduction

Researchers' interest in porous metallic materials is growing as a means of minimizing mechanical incompatibilities between bulk metallic implants and the natural bone. The stress shielding effect is started by these mechanical mismatches, which result in inadequate loading of the bone [1]. It ultimately results in implant loosening and bone resorption. Therefore, a metallic implant with a porous structure was created to address this problem. Additionally, by allowing mechanical interlock with the porous structure through bone ingrowth, the porous structure can promote osseointegration and provide stable long-term fixation [2].

Titanium and its alloys, in particular for loading-bearing applications, are promising materials utilized for bone implants. Because of its high mechanical properties, robust corrosion resistance, and biocompatibility, Ti-6Al-4V is often utilized for dental implants [3]. When it comes to materials, titanium and its alloys are attractive choices for bone implants, particularly in load-bearing applications. Due to its high mechanical qualities, superior corrosion resistance, and biocompatibility, Ti-6Al-4V is frequently utilized for dental implants [3]. The process of creating a highly porous dental implant, which includes freeze casting and fast prototyping, has been the subject of much research. Freeze casting is able to manufacture Ti-6Al-4V dental implants with high aspect ratio pores, but it also results in excessive oxygen contents and poor mechanical properties [4], [5]. While rapid prototyping is a method that uses three-dimensional computer-aided design to quickly create a scale model of a part or

assembly. The produced model, however, occasionally exhibited defects including unmelted powders, inclusions, and impurities that might impair its mechanical qualities [6], [7].

Alternative technologies like metal injection molding (MIM) may produce components with near-net shapes, a variety of sizes, and complicated geometries while yet having high mechanical qualities. Starting with the mixing of the metallic powder with binders and space holders to create a uniform feedstock, MIM consists of four basic phases [8], [9]. The pore structure created in the dental implant is determined by the space holder. In the second stage, the feedstock is injected into the mold to create a green body. The third stage involves removing the space holder and binders from the green body. The sintering process, in which the brown body or final component were created, is the fourth and last stage [10]-[13]. The aim of the present study was to investigate the surface structure and morphology of three different powder loading of Ti-6Al-4V dental implants.

2. Methodology

2.1 Samples Preparation

The Ti-6Al-4V metal powder employed in this study has a spherical shape and an average size of 18µm and was produced by gas atomizing. The Ti-6Al-4V metal powder used in this work is described in Table 1 with its properties, and its chemical composition is shown in Table 2. Fig. 1 exhibits spherical Ti-6Al-4V powder under the scanning electron microscope (SEM). Fig. 2 shows the schematic diagram of the Ti-MIM tensile bar with thickness of 2.7 mm. Two types of binder were used which are 60wt% of palm stearin (PS) and 40wt% of polyethylene (PE). The space holder material used were NaCl with particle size of <100µm. NaCl was chosen as space holder because it is an inorganic compound which can be easily dissolved in water and removed during the MIM process to produce desirable porosity [10]. Three different powder loading were evaluated: 63vol%, 64vol% and 65vol%. All materials were mixed together by using sigma blade mixer at temperature of 150°C. Once the homogenized granules of feedstock were obtained, it was injected into the dental screw mold using vertical injection molding. Two stages of debinding process were solvent extraction and water leaching. The injected samples were immersed in the heptane solutions for 6 hours at 60°C to remove palm stearin. Afterward, it was immersed in distilled water for water leaching at 40°C to remove NaCl. Removals of PE were done in one furnace during sintering on 500°C then continue sintered up to 1200°C.

Table 1 *Ti-6Al-4V powder physical properties*

Particle size distribution (µm)			Pycnomete density (g/cm^3)	Melting Temperature (°C)
D_{10}	D_{50}	D_{90}		
11.2	18.8	30.5	4.38	1650

Table 2 *Chemical composition of Ti-6Al-4V powder*

Al	V	C	Fe	O	N	H	Ti (wt%)
5.99	4.08	0.005	0.043	0.185	0.004	0.002	Bal

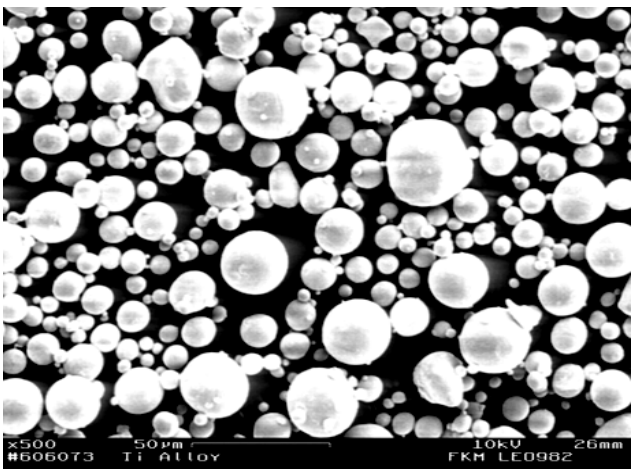

Fig. 1 *SEM Ti-6Al-4V powder*

Int. Journal of Integrated Engineering Vol. 16 No. 8 (2024) p. 227-235

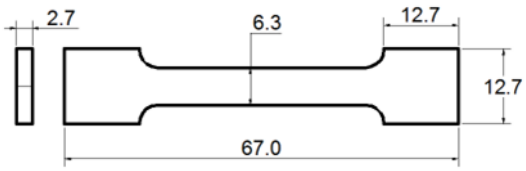

Fig. 2 *Injection mold part and geometry (Dimensions are in mm)*

2.2 Thermal Debinding and Sintering Process

Two stages of debinding process were solvent extraction and water leaching. The injected samples were immersed in the heptane solutions for 6 hours at 60°C to remove palm stearin. Afterward, it was immersed in distilled water for water leaching at 40°C to remove NaCl. Removals of PE were done in one furnace during sintering on 500°C then continue sintered up to 1200°C. Thermal debinding and sintering process was carried out once the samples were dried and weighed after the solvent debinding process. Thermal debinding and sintering was performed in the same furnace which was KOREA VAC-TEC high temperature control atmosphere furnace as can be seen in Fig. 3. The vacuum pressure of this furnace can achieve up to 10^{-6} torr to eliminate any impurities during the experiment.

The debound samples were placed on an aluminate plate and put into a Molybdenum (Mo) box as shown in Fig. 4. It was done to prevent chemical reaction of residual binder to the heating element of the furnace, thus, secure the heating process. Thermal debinding and sintering parameters such as heating rate, temperature, soaking time and cooling rate were set based on the study of thermal debinding and sintering parameter optimization done by Abu Kassim et al. [5]. In order to reduce trial and error procedures, a preliminary thermal debinding and sintering process were performed. After a few trials, only parameter of thermal debinding heating rate was selected to be resolved for best as-sintered parts results assessment. Fig. 5 shows the profile and the parameter of thermal debinding and sintering process respectively.

Fig. 3 *KOREA VAC-TEC high temperature control atmosphere furnace*

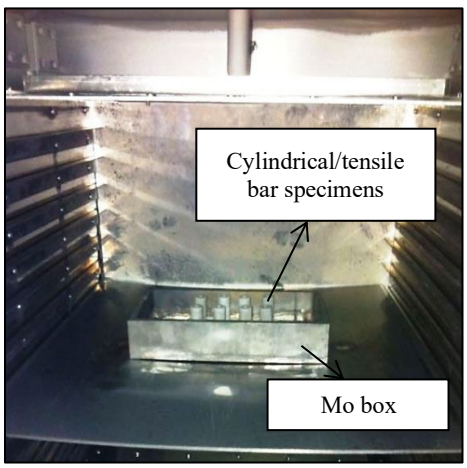

Fig. 4 *The samples were loaded into the furnace*

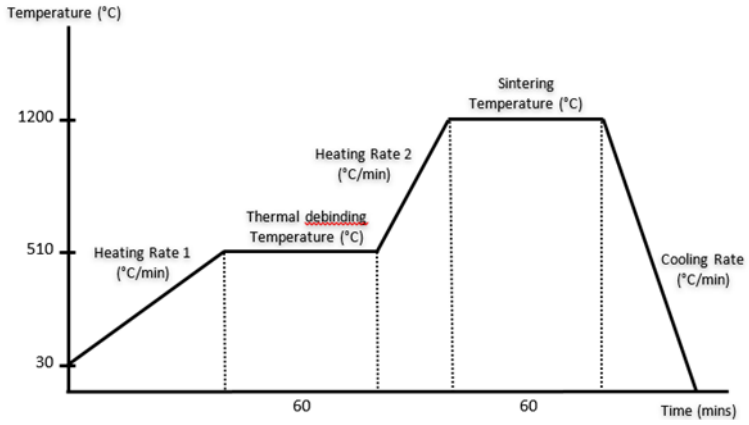

Fig. 5 *Thermal debinding and sintering profile*

2.3 Samples Characterization

Scanning Electron Microscopy (SEM) was used in order to observe the microstructure of the as-sintered samples. A non-contact optical profilometry was used to measure the surface roughness of the as-sintered samples.

3. Results and Discussion

In order to fabricate a porous Ti-6Al-4V, NaCl is employed in this study as the space holder to produce sufficient network of pores. NaCl was selected because it easily dissolved in water, inexpensive, and lower toxicity [6]-[8]. The morphology of NaCl observed under SEM at 300x magnification as shown in Fig. 6 has confirmed that the shape of space holding particles is irregularly shaped. Based on Fig. 6, the sieved NaCl distribution size was around 150µm to 300µm. Sieved space holder is more preferable to obtain a narrow distribution of space holding particles which resulted in better mechanical strength to the porous structure [8].

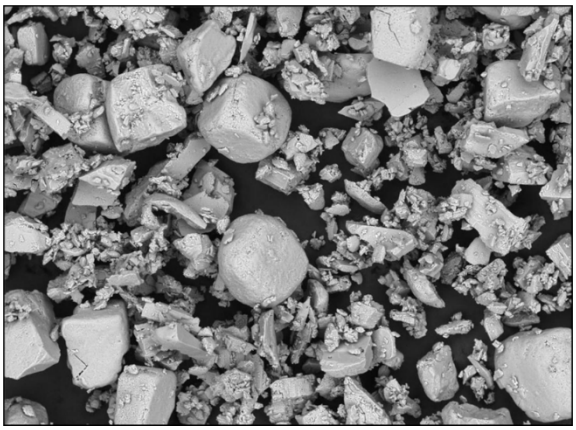

Fig. 6 *SEM observation of NaCl as the space holder*

The 150-300µm size of NaCl particles was chosen to promote interconnectivity of the pores formed after sintering as well as to produce adequate mechanical strength. There was bigger size range of NaCl used in other study such as Alejandra et al. [9] used NaCl in the range of 355µm to 500µm to fabricate porous Ti structure via MIM. However, the mechanical strength values of the as-sintered parts recorded was low. So, in this work, medium sized range of NaCl was selected to produce sufficient network of interconnected pores that would result in better mechanical properties. Fig. 7 shows the distribution of powder and binder after mixing process that demonstrates the homogenous feedstock. It can be seen in Fig. 7, PE enveloped the Ti-6Al-4V metal powder particles and both of them cover thoroughly NaCl particles since NaCl has the biggest size in the mixture components. No agglomeration of metal powder particles show that the feedstocks produced was mixed homogenously.

Successes of dental implants are governed by cellular response to the characteristics of the implant surface [14]. Topography of the dental implant surface was revealed by scanning electron microscopy (SEM), as shown in Fig. 8. The SEM image showed that the surface of the dental was roughened. The porosity structure obtained also randomly distributed within the dental implant. The pores structure is in non-uniformly shape with existence of the integrated pores which is very accommodating for the osseointegration process. The integrated pores would provide the space for mineralized bone to growth and diffuse into the dental implant. It also improves the

Int. Journal of Integrated Engineering Vol. 16 No. 8 (2024) p. 227-235

anchorage of the dental implant towards the bone which lead to the prevention of dental implant loosening [11], [12].

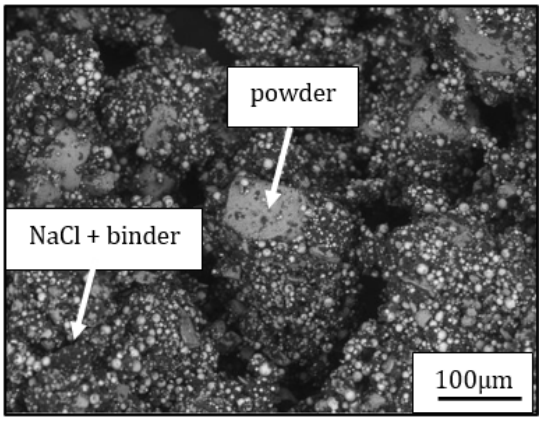

Fig. 7 *SEM of homogenous feedstock*

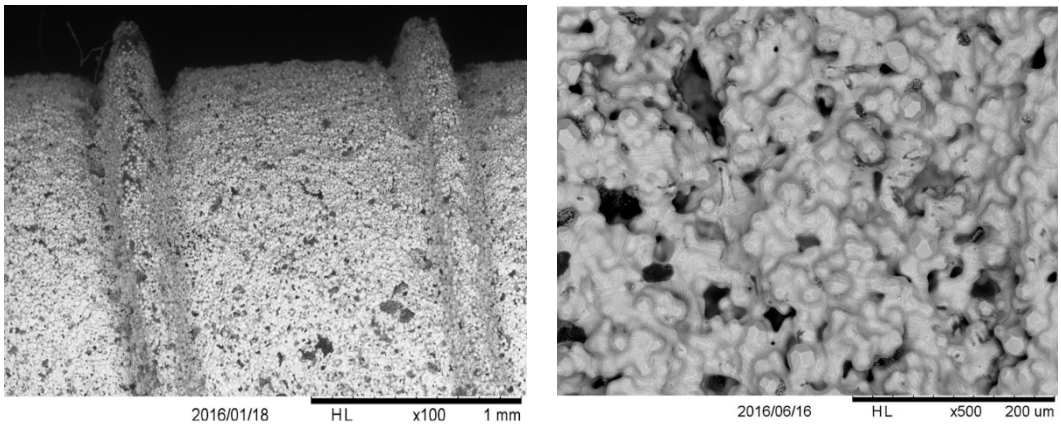

(a) **(b)**

Fig. 8 *SEM of the dental implant surface: (a) Low magnification view (100x, bar:1mm); (b) Threaded surface at high magnification (500x, bar:200µm)*

Dental implant morphology influences bone metabolism: rougher surfaces stimulates differentiation, growth and attachment of bone cells, and increases mineralization. Furthermore, the degree of roughness is important. It is reported that the micro topographic profile of dental implants is defined for surface roughness as being in the range of 1-10µm [15]. Surface roughness values obtained for the dental implant are listed in Table 3. As the data shown in Table 3, the surface roughness (Ra) obtained a mean value of 4.62 ± 1.33 µm to 5.83 ± 1.25 µm which is within the range. This range of roughness maximize the interlocking between mineralized bone and the surface of the implant. It is also suggested that theoretically, the ideal surface should be covered with hemispherical pits approximately 1.5µm in depth and 4µm in diameter [16].

Table 3 *Average surface roughness (Ra) of different powder loading*

Samples	Ra (in µm)
Powder loading 63vol %	4.62 ± 1.33
Powder loading 64vol %	5.12 ± 1.28
Powder loading 65vol%	5.83 ± 1.25

From the microscopic observation, some of the micropores were observed on the surface of the as-polished specimen as shown in Fig. 9. This could be caused by the effect of partially sintering of Ti-6Al-4V metal powders on the pore walls [17]. Moreover, the micropores formation may also be induced by the debris of NaCl which was broken during the mixing process and formed micropores after water leaching process.

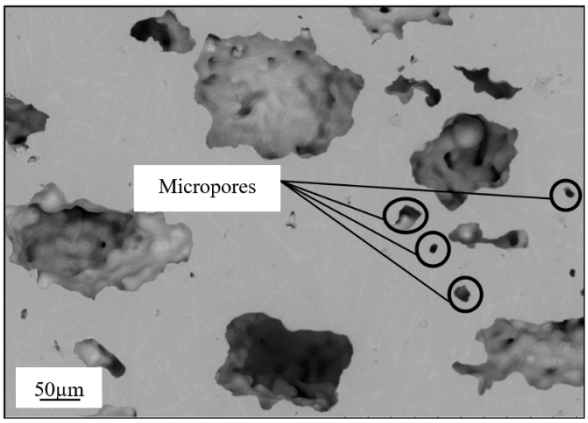

Fig. 9 *Micropores observed on the as-polished specimens*

The interconnected pore structure is favourable to promote ingrowth of new bone tissues and fluid transport [18]. Sharma et. al [19] stated that the evolution of isolated pores to interconnected pores happened when the total porosity of porous structure achieved to 55%. However, such statement is contrary to the microscopic observation in this experiment. Although the porosity percentage is less than 50%, the inter-connection among the pores formed was clearly observed under FESEM as shown in backscattered images in Fig. 10. The figures were taken from the cross section of the tensile body of 63, 64 and 65 vol.% specimen. This could be due to the fact that the uniformity of mixture contributed by the PS binder has provided homogenous distribution of space holder in the feedstocks [20]. This factor has led to better pore distribution which increased the interconnectivity among the pores.

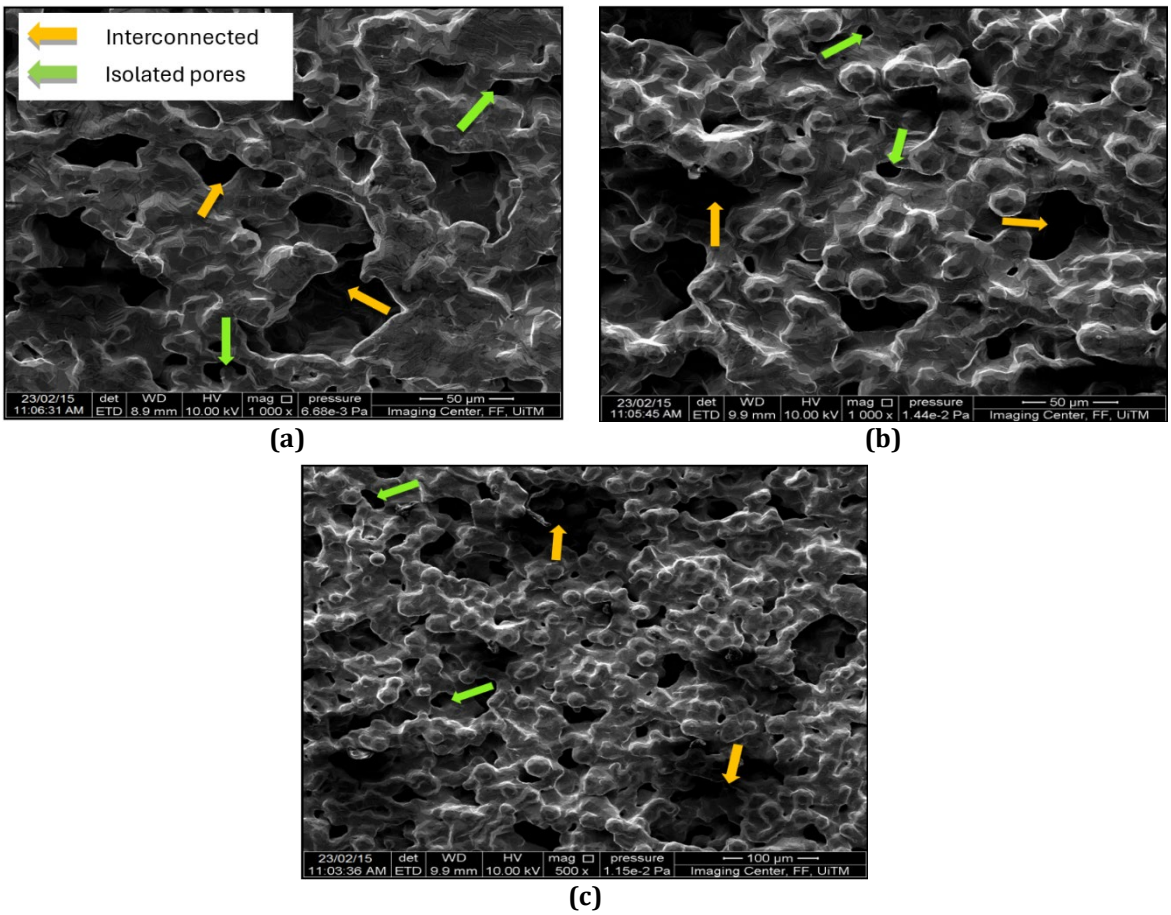

Fig. 10 *The example of interconnected pores and isolated pores in the as-sintered specimens for: (a) 63vol.%; (b) 64vol.%; and (c) 65 vol.%*

However, there are some isolated pores that are present which replicates the shape of NaCl. Based on the scale of the Fig. 10, most of the isolated pores have the size less than 50µm due to the effect of pores annihilation.

Int. Journal of Integrated Engineering Vol. 16 No. 8 (2024) p. 227-235

Pores annihilation was induced by the enlargement of grain growth during the sintering process. This phenomenon can be seen on the as-polished sample where the pore was disrupted by the growth of the grain as shown in Fig. 11.

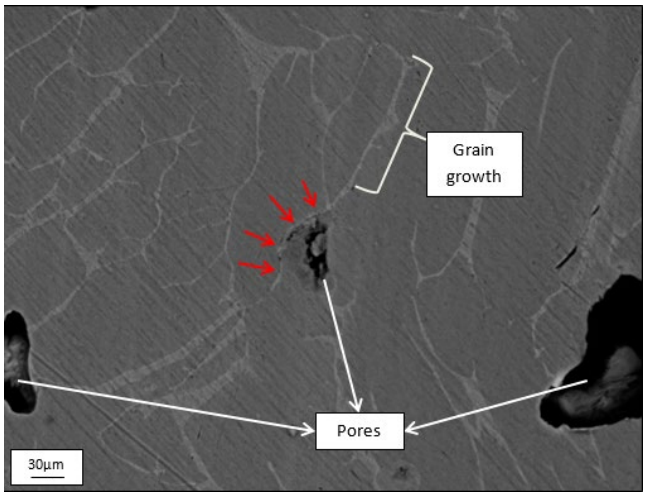

Fig. 11 *Red arrows show one of the pores was disrupted due to enlargement of grain growth on the as-polished sample*

The goal of microstructure analysis is to ascertain the phase developed in the as-sintered specimen is the phase of Ti-6Al-4V without the presence of other interstitial elements. Aluminium is an α-stabilizer and Vanadium is a β-stabilizer for Ti-6Al-4V phase [21]. As the processing route of MIM applies high temperature to melt down the Ti-6Al-4V metal powder particles during sintering, less primary α and more β were present in terms of retained β and transformation α (β→α) phase on the surface of the as-sintered specimen [22].

Fig. 12 depicts the presence of lamellae of α on the surface of the as-polished sample at 500x magnification. The presence of lamellae of α demonstrates that the transformation α (β→α) phase has separated the globular α and appears in terms of typical (α+β) phase of Ti-6Al-4V [23]. Thus, the presence of typical (α+β) phase as displayed in Fig. 12 has confirmed the morphology of Ti-6Al-4V phase.

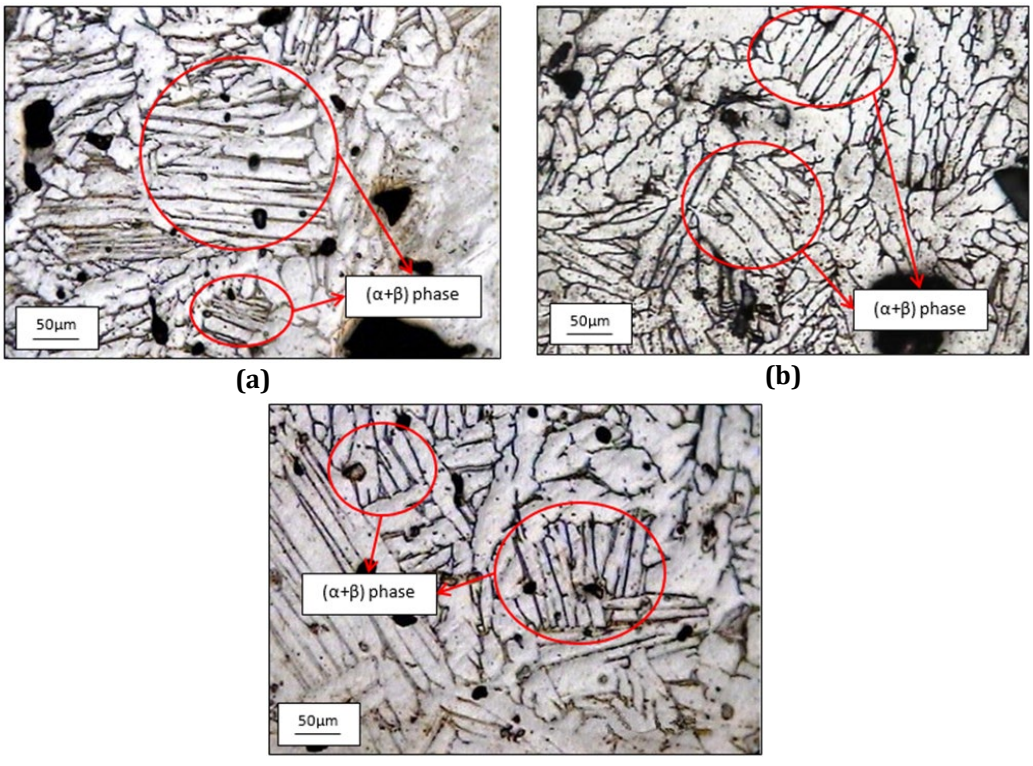

Fig. 12 *The presence (α+β) phase shown on the surface of as-polished porous Ti-6Al-4V sample for (a) 63 vol.%; (b) 64 vol.%; and (c) 65 vol.% powder loading specimens*

4. Conclusions

In conclusion, porous Ti-6Al-4V dental implant fabricated through MIM with palm stearin binder system showed a potential method in producing a suitable surface characteristic in enhancing the osseointegration purpose. The average surface roughness (Ra) of 4.62 ± 1.33 μm and 5.83 ± 1.25 μm was within the proposed ideal surface roughness (1-10μm) to stimulate the growth and attachment of bone cells. Further study for the biocompatibility on the surface of the dental implant would help a better understanding on the growth attachment of the bone cells. In terms of microstructural analysis, the pores of porous structures for all specimens are not fully interconnected. Some of the pores were isolated and some of the pores were eliminated due to densification during the sintering process. The pores shape was irregular replicating the geometry of NaCl.

Acknowledgement

The author would like to thank Universiti Teknologi MARA (UiTM) for awarding the research grant 600-IRMI/PERDANA 5/3 BESTARI (043/2018) to conduct the present research. Many thanks also to Universiti Kebangsaan Malaysia for providing MIM equipment.

Conflict of Interest

Authors declare that there is no conflict of interest regarding the publication of the paper.

Author Contribution

The authors confirm contribution to the paper as follows: ***study conception and design:*** *J. B. Saedon, N. H. Mohamad Nor;* ***data collection:*** *N. H. Mohamad Nor, M. H. Ismail;* ***analysis and interpretation of results:*** *N. H. Mohamad Nor, Hazran Husain;* ***draft manuscript preparation:*** *M. Newishy. All authors reviewed the results and approved the final version of the manuscript.*

References

[1] Dehghan-Manshadi, A., Yu, P., Dargusch, M., StJohn, D. & Qian, M. (2020). Metal injection moulding of surgical tools, biomaterials and medical devices: A review. Powder Technology, 364, 189-204. https://doi.org/10.1016/j.powtec.2020.01.073

[2] Yuan, L., Ding, S. & Wen, C. (2019). Additive manufacturing technology for porous metal implant applications and triple minimal surface structures: A review. Bioactive Materials, 4, 56-70. https://doi.org/10.1016/j.bioactmat.2018.12.003

[3] Zheng, J. P., Chen, L. J., Chen D. Y., Shao, C. S., Yi, M. F. & Zhang, B. (2019). Effects of pore size and porosity of surface-modified porous titanium implants on bone tissue ingrowth. Transactions of Nonferrous Metals Society of China, 29, 2534-2545. https://doi.org/10.1016/S1003-6326(19)65161-7

[4] Song, C., Liu, L., Deng, Z., Lei, H., Yuan, F., Yang, Y., Li, Y. & Yu, J. (2023). Research progress on the design and performance of porous titanium alloy bone implants. Journal of Materials Research and Technology, 23, 2626-2641. https://doi.org/10.1016/j.jmrt.2023.01.155

[5] Abu Kasim, N. A., Mohamad Nor, N. H., Ismail M. H. & Saedon, J. (2017). Development of porous Ti-6Al-4V dental implant by metal injection molding with palm stearin binder system. Materials Science Forum, 889, 79-83. https://doi.org/10.4028/www.scientific.net/MSF.889.79

[6] Ray, S., Jana, P., Kar, S. K. & Roy, S. (2023). Influence of monomodal K2CO3 and bimodal K2CO3 + NaCl as space holders on microstructure and mechanical properties of porous copper. Materials Science and Engineering: A, 862, 144516. https://doi.org/10.1016/j.msea.2022.144516

[7] Zakaria, M. Y., Ramli, M. I., Sulong, A. B., Muhamad, N. & Ismail, M. H. (2021). Application of sodium chloride as space holder for powder injection molding of alloy Titanium–Hydroxyapatite composites. Journal of Materials Research and Technology, 12, 478-486. https://doi.org/10.1016/j.jmrt.2021.02.087

[8] Aida, S.F., Hijrah, M.N., Amirah, A.H., Zuhailawati, H. & Anasyida, A. S. (2016). Effect of NaCl as a space holder in producing open cell A356 aluminium foam by gravity die casting process. Procedia Chemistry, 19, 234-240. https://doi.org/10.1016/j.proche.2016.03.099

[9] Rodriguez-Contreras, A., Punset, M., Calero, J. A., Gil, F. J., Ruperez, E. & Manero, J. M. (2021). Powder metallurgy with space holder for porous titanium implants: A review. Journal of Materials Science & Technology, 76, 129-149. https://doi.org/10.1016/j.jmst.2020.11.005

[10] Liu, Y., Pan, Y., Sun, J., Wu, X., Zhang, J., Kuang, F. & Lu, X. (2023). Metal injection molding of high-performance Ti composite using hydride-dehydride (HDH) powder. Journal of Manufacturing Processes, 89, 328-337. https://doi.org/10.1016/j.jmapro.2023.01.064

[11] Kultamaa, M., Mönkkönen, K., Saarinen, J. J. & Suvanto, M. (2022). Self-lubrication of porous metal injection molded (MIM) 17-4PH stainless steel by impregnated paraffin wax. Tribology International, 174, 107735. https://doi.org/10.1016/j.triboint.2022.107735
[12] Sidambe, A. T., Todd, I. & Hatton, P. (2015). Effect of processing parameters on the properties of metal injection moulded titanium dental implants. Materials Science Forum, 828–829, 145–151. https://doi.org/10.4028/www.scientific.net/MSF.828-829.145
[13] Hayat, M. D., Jadhav, P. P., Zhang, H., Ray, S. & Cao, P. (2018). Improving titanium injection moulding feedstock based on PEG/PPC based binder system. Powder Technology, 330, 304-309. https://doi.org/10.1016/j.powtec.2018.02.043
[14] Hoque, M. E., Showva, N. N., Ahmed, M., Rashid A. B., Sadique, S. E., El-Bialy T. & Xu, H. (2022). Titanium and titanium alloys in dentistry: current trends, recent developments, and future prospects. Heliyon, 8, E11300. https://doi.org/10.1016/j.heliyon.2022.e11300
[15] Soares, F. M. S., Barbosa, D. M., Corado, H. P. R., Santana A. I. C. & Elias, C. N. (2022). Surface morphology, roughness, and corrosion resistance of dental implants produced by additive manufacturing. Journal of Materials Research and Technology, 21, 3844-3855. https://doi.org/10.1016/j.jmrt.2022.10.114
[16] Ren, B., Wan, Y., Liu, C., Wang, H., Yu, M., Zhang, X. & Huang, Y. (2021). Improved osseointegration of 3D printed Ti-6Al-4V implant with a hierarchical micro/nano surface topography: An in vitro and in vivo study. Materials Science and Engineering: C, 118, 111505. https://doi.org/10.1016/j.msec.2020.111505
[17] Fujii T., Murakami, R., Kobayashi, N., Tohgo, K. & Shimamura, Y. (2022). Uniform porous and functionally graded porous titanium fabricated via space holder technique with spark plasma sintering for biomedical applications. Advanced Powder Technology, 33, 103598, https://doi.org/ 10.1016/j.apt.2022.103598
[18] Torres-Sanchez, C., McLaughlin, J. & Fotticchia, A (2018). Porosity and pore size effect on the properties of sintered Ti35Nb4Sn alloy scaffolds and their suitability for tissue engineering applications. Journal of Alloys and Compounds, 731, 189-199. https://doi.org/10.1016/j.jallcom.2017.10.026
[19] Sharma, M., Gupta, G. K., Modi, O. P., & Prasad, B. K. (2013). PM processed titanium foam: influence of morphology and content of space holder on microstructure and mechanical properties. Powder Metallurgy, 56, 55-60. https://doi.org/10.1179/1743290112Y.0000000036
[20] Arifvianto, B. & Zhou, J. (2014). Fabrication of metallic biomedical scaffolds with the space holder method: A Review. Materials, 7, 3588-3622. https://doi.org/10.3390/ma7053588
[21] Huang, S., Zhao, Q., Wu, C., Lin, C., Zhao, Y., Jia, W. & Mao, C. (2021). Effects of β-stabilizer elements on microstructure formation and mechanical properties of titanium alloys. Journal of Alloys and Compounds, 876, 160085. https://doi.org/10.1016/j.jallcom.2021.160085
[22] Wanhill, R. & Barter, S. (2012). Fatigue of Beta Processed and Beta Heat-Treated Titanium Alloys. Springer Dordrecht. https://doi.org/10.1007/978-94-007-2524-9
[23] Obasi, G. C., Ferri, O.M., Ebel, T. & Bormann, R. (2010). Influence of processing parameters on mechanical properties of Ti–6Al–4V alloy fabricated by MIM. Materials Science and Engineering: A, 527, 3929-3935. https://doi.org/10.1016/j.msea.2010.02.070